Half-Metallicity Properties of Hexagonal Monolayer Slab of Graphene-Like ZnX (X = S, Se) Monolayers Doped with Transition Metals

Received: 16.01.2021 & Accepted: 13.04.2021

A. Mohammadi[a], A. Avazpour[a,*] and M. Moradi[b]

[a] *Physics Department, Faculty of Science, Yasouj University, Yasouj, Iran*
[b] *Department of Physics, Faculty of Science, Shiraz University, Shiraz, Iran*

Doi: 10.12693/APhysPolA.139.679 *e-mail: avazpour@yu.ac.ir

In this work, the density functional theory is employed to study the electronic and magnetic properties of Y(Fe,Co,Mn,Ni) doped ZnX (X = S, Se) hexagonal monolayers. The transition metal dopants are substituted in two different positions. The calculated results show that the magnetic properties of the ZnX monolayer can be tuned by changing the kind and distribution of impurities. The Mn and Ni doping does not show polarity and half-metallic property. In the structures doped with Fe and Co, we observed the 100% spin polarity and half-metallic property. Our findings suggest that the doping with the transition metals in this kind of monolayers is a suitable scheme for a future design of transition metal dichalcogenides as a based target in technological applications.

topics: half-metallic, spintronic, magnetic properties

1. Introduction

With the development of smaller transistors in the last decades, electronic technology has made great strides. However, by reducing the size of transistors, scientists theoretically and experimentally reached the size limit due to the quantum mechanics limit. In order to continue the development, there is a need of developing new materials with suitable electronic properties that can replace the silicon-based electronics used nowadays. Graphene, a new two-dimensional (2D) material, as a single layer of graphite, has become the focus of research for producing breakthroughs in many areas over the last two decades [1, 2]. Graphene has been proposed for a variety of applications due to its unique physical properties, especially as an alternative to silicon-based electronic applications [3–6]. However, graphene is not suitable for the fabrication of the field-effect transistors (used in logical applications), due to its lack of an inherent band gap [6–8]. This has led to a search for other two-dimensional materials with a suitable band gap and similar properties.

The graphene-like materials can show special magnetic property when doped with magnetic impurities. For example, they can be semi-metallic, semi-ferromagnetic or ferromagnetic semiconductors [9, 10]. Among the graphene-like inorganic materials known to date, one of the best-known representatives are monolayers of transition metal dichalcogenides (TMDs). The TMDs are the materials of form MX_2 where M is a transition metal e.g., Mo, W, V, Nb, and X is a chalcogen, e.g., S, Se, Te [8]. Among the two-dimensional TMDs, some of them show a semiconducting behavior with a band gap in the visible spectrum (e.g., MoS_2), which makes them suitable for field-effect transistors and optoelectronics [8–11]. In order to find and study the materials with proper electrical properties, a wide range of theoretical and experimental methods is used. The most commonly used method for theoretical calculations is the density functional theory, DFT, a method where the electronic structure is described as a functional of the electron density [12].

Recently, many theoretical and experimental studies have focused on the magnetic properties of graphene-like materials such as 1H-MoS_2 [13–16]. The bulk structure of MoS_2 is composed of two molecular layers of MoS_2 with a trigonal prismatic phase named as 2H-MoS_2. The mechanical method always leads to a 2D trigonal prismatic phase — commonly denoted as 1H-MoS_2 — and found to be a semiconductor with a direct 1.80 eV band gap, as opposed to graphene's zero energy gap. Thus, the magnetic doping by adsorption or substitution became an effective method of magnetism induction in non-magnetic MoS_2 and similar compounds [17–20]. For example, magnetic interactions can be tuned by carriers and strain. At the same time, it was found that the sulfur S vacancies are related to the magnetic properties of MoS_2 [21]. These vacancies not only affect the magnetic properties, but also change

the density of the semiconductor carrier. Obviously, S vacancies can affect magnetism when doped with transition metals. Many studies have been reported on each of these two findings [22–28]. However, it is not clear how these two aspects interplay and what is the influence of this interplay on the magnetic properties.

In this paper, the DFT theoretical methods are used to study the effect of group VIII transition metals atom doping on the ZnX (X = S, Se) compounds. Due to the fact that these compounds have shown magnetic properties in various crystal structures by adding impurities, they can be considered as a suitable option [29–32]. We design the doped slab of a hexagonal structure of ZnX materials to consider their electronic and magnetic properties using the first-principle calculations. This study proposes a new idea of ferromagnetism as a half-metallic material for spin valves and spintronic applications.

2. Computational method

Our calculations are performed on the basis of the spin polarized density functional theory as applied in the QUANTUM ESPRESSO first principles simulation package [33]. We have used the PWscf code for solving the Kohn–Sham equations self-consistently and obtaining optimized parameters. The pseudopotentials are used to represent the electron–ion interactions. We used ultra-soft pseudopotentials with the generalized gradient approximation, GGA, in the exchange-correlation interaction which proposed by Perdew, Burke and Ernzerhof (PBE96) [34].

In these calculations, a $4 \times 4 \times 1$ ZnX supercell structure containing 16 atoms of Zn and X (X = S, Se) was constructed as the pristine model. Moreover, a vacuum region of 10 Å was added along the c direction to minimize the interaction between the adjacent periodic images. The cutoff energy for the plane-wave expansion is set to be 250 eV after extensive convergence analysis. The Brillouin zone (BZ) is sampled using $3 \times 3 \times 1$ gamma-centered Monkhorst–Pack grid. The valence electron configurations in these calculations are $4p^6 4d^5 5s^1$, $3s^2 3p^4$, $4s^2 4p^4$, $3d^6 4s^2$, $3d^7 4s^2$, $3d^8 4s^2$, $3d^5 4s^2$ for Zn, S, Se, Fe, Co, Ni and Mn, respectively. All of the arrangements are fully relaxed during the structural relaxation, the energy convergent criterion is 10^{-6} eV per unit cell and the forces on all relaxed atoms are less than 10^{-4} eV/Å.

3. Results and discussion

3.1. Optimized geometric structure

In this work, the focus is on the hexagonal structure of the ZnS and ZnSe compounds, which are impure by the elements of group VIII transitional metals. To simulate the doped transitional metal

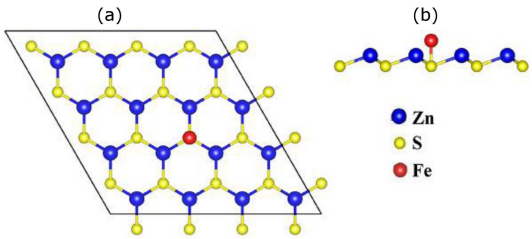

Fig. 1. Top (a) and side (b) views of the supercell configuration for the doped $4 \times 4 \times 1$ ZnS monolayer by the Fe atom dopant on the top of the supercell.

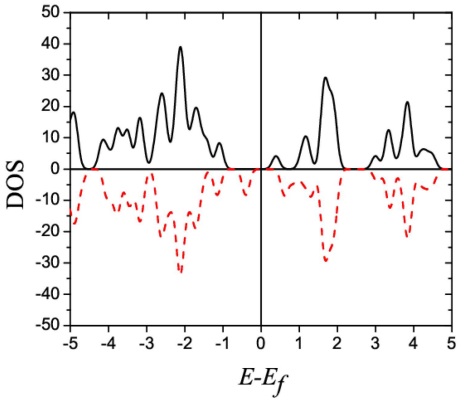

Fig. 2. Density of states of the ZnS monolayer by the Fe atom dopant on the top of the supercell, black solid and red dashed lines, is related to spin up and spin down states, respectively. Both the spin up and spin down channels have an energy gap around the Fermi energy.

structures, a $4 \times 4 \times 1$ supercell was adopted. In preliminary efforts, we considered various structures and scenarios, including placing the doping atom on top of the structure. For instant, in one scenario, we placed the Fe atom above the surface of the hexagonal monolayer structure (Fig. 1a and b). This atom was placed 4 Å above the S atom. The structure was optimized by minimizing the applied force. The calculated DOS of this structure is shown in Fig. 2. Both the spin up and spin down channels have an energy gap around the Fermi energy. Also, supercell magnetization of this system was equal to $2\mu_B$. As a result, the structure was considered a magnetic semiconductor [13, 29]. Because our purpose was to achieve structures with half-metallic properties, this scenario was set aside for future studies. We further opted for the substitution as the main focus of our search for half-metallic structure (see Fig. 3).

As shown in Fig. 3, one Zn, S or Se atom was replaced by one transitional metal atom with the doping concentration of 6.25%. The geometrical structures and atom positions were fully relaxed. The four elements of Fe, Mn, Co and Ni have been added separately in two spatially different positions.

TABLE I

The optimized parameters for pure ZnS, ZnSe and the doped monolayers in different configurations. The total energy, formation energy, Fermi energy, total magnetic moment and half-metallic energy band gap are shown.

Doped atom	Configurations	Position of doped atoms	$E_{\rm tot}$ [Ry]	$E_{\rm form}$ [eV]	$E_{\rm F}$ [eV]	$M_{\rm tot}$ [$\mu_{\rm B}$]	$E_{g-{\rm half}}$ [eV]
ZnS-doped							
–	ZnS	–	−2353.8	–	−0.9636	0.00	–
Fe	$Zn_{15}FeS_{16}$	A	−2282.9	−36.34	−0.5769	4.00	0.777
	$Zn_{16}S_{15}Fe$	D	−2388.7	−103.84	−0.0554	2.00	1.536
Co	$Zn_{15}CoS_{16}$	A	−2301.5	−44.00	−1.3648	3.00	0.124
	$Zn_{16}S_{15}Co$	D	−2407.4	−89.01	−0.4670	1.00	0.942
Mn	$Zn_{15}MnS_{16}$	A	−2436.4	−101.91	−0.7934	5.00	–
	$Zn_{16}S_{15}Mn$	D	−2542.2	−232.6	−0.2711	3.00	–
Ni	$Zn_{15}NiS_{16}$	A	−2313.0	−48.75	−1.3458	2.00	–
	$Zn_{16}S_{15}Ni$	D	−2418.9	−166.6	−0.3911	0.00	–
ZnSe-doped							
–	ZnSe	–	−2326.1	–	−0.3860	0.00	–
Fe	$Zn_{15}FeSe_{16}$	A	−2255.3	−36.33	−0.4993	4.00	0.643
	$Zn_{16}Se_{15}Fe$	D	−2362.8	−99.92	0.0249	2.00	1.397
Co	$Zn_{15}CoSe_{16}$	A	−2273.9	−43.99	−1.1396	3.00	–
	$Zn_{16}Se_{15}Co$	D	−2381.5	−107.6	−0.3549	1.00	1.011
Mn	$Zn_{15}MnSe_{16}$	A	−2408.5	−101.89	−0.3909	5.00	–
	$Zn_{16}Se_{15}Mn$	D	−2516.3	−165.46	−0.1065	3.00	–
Ni	$Zn_{15}NiSe_{16}$	A	−2285.4	−48.75	−1.1890	2.00	–
	$Zn_{16}Se_{15}Ni$	D	−2393.1	−122.39	−0.1572	0.00	–

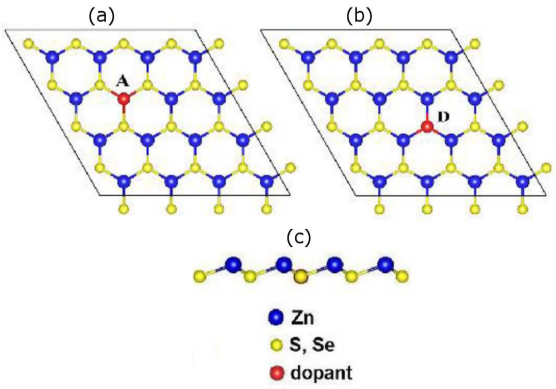

Fig. 3. Top (a) and (b), and side (c) views of the supercell configuration for the doped $4 \times 4 \times 1$ ZnX monolayer. Two different configurations of dopants are taken into account in this work with the marked positions of A and D.

These two positions are also shown in Fig. 3. The site A represents the position of the Zn atom, and the D site represents the S or Se atoms, where the dopant atoms are substituted in all of them separately. We used force minimization with 10^{-4} eV/Å convergence limits to optimize the structure. All doped systems maintain in the original structure-type of ZnX monolayer, albeit with a slight lattice distortion owing to the 3*d* TM substitution. The distortion is due to a smaller ion radius of 3*d* TM substitution than Zn, S, and Se.

The obtained total energies per chemical formula as a function of lattice constant are illustrated in Fig. 4. When the lattice constant of ZnS is 3.8 Å, and of ZnSe is 3.98 Å, then the energies are minimized. The minimum total energy shows that the structure reaches a steady state and, the applied force to the atoms in the structure is the lowest. The minima of the total energies per chemical formula for all stable configurations are given in Table I.

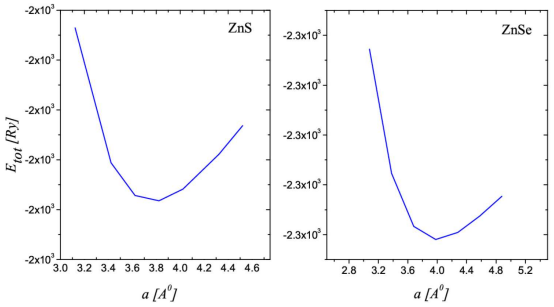

Fig. 4. Total energy of ZnS and ZnSe versus the lattice constant in the pure case.

In order to consider the stability of the given structures, we performed the calculations related to the formation energy [35] according to:

$$E_{\text{form}} = E_{\text{doped}} - E_{\text{pure}} + \mu_{\text{host}} - \mu_{\text{doped}}, \quad (1)$$

where E_{doped} and E_{pure} represent the total energies of the transitional metal doped ZnS (ZnSe) monolayer and the pure monolayer, respectively. Also, μ_{host} and μ_{doped} are the chemical potentials for the Zn (S) hosts and the transitional metal dopant atoms, respectively. All formation energies are listed in Table I.

3.2. Electronic properties of ZnX (X=S, Se) monolayer

In order to determine the initial properties of the ZnS and ZnSe compounds without a dopant, first we performed the calculations of their electronic structure. To have better insight into the magnetic behavior, the density of states (DOS) of both monolayers is shown in Fig. 5. As indicated by blue dotted lines, the Fermi level is set at zero energy for easier identification of the band gap [36] and the relative position of the states from the impurity atoms.

The density of states shows the semiconductor property for the undoped ZnS and ZnSe since there are energy gaps in two spin channels. On the other hand, according to Table I, their total magnetic moments are zero and they do not show magnetic properties in general. Also, the valence band maximum is at $(E - E_{\text{F}})$ value, i.e., -2.2 eV for ZnS and -2.0 eV for ZnSe (where E_{F} is the Fermi energy). This is mainly due to electronic transitions between the $3d$ orbitals of Zn and the $3p$ orbitals of S and Se. The other peaks from -1.0 to -2.2 eV and -0.7 to -2.0 eV for ZnS and ZnSe are also associated with the $3p$ orbitals of S and the $4s$ orbitals of Zn. The precise mirror symmetry between the spin up and spin down states indicates

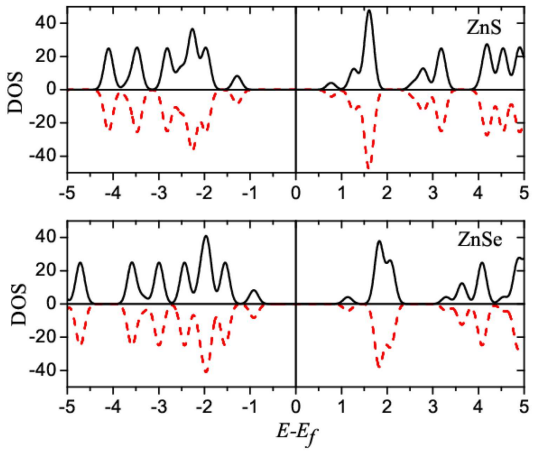

Fig. 5. Densities of states of ZnS and ZnSe monolayers, black solid and red dashed lines, are related to spin up and spin down states, respectively.

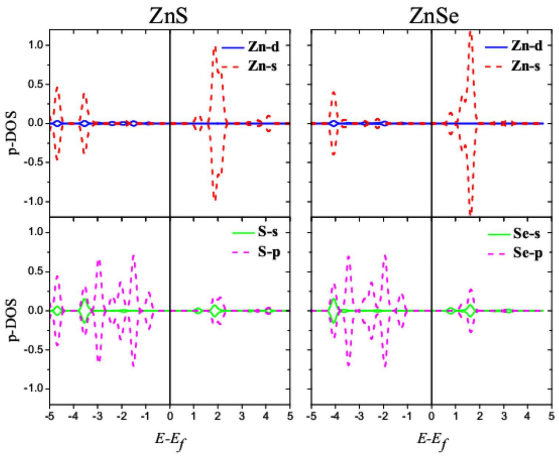

Fig. 6. The calculated partial DOS of the Zn and the S (Se) atoms in the pure ZnS and ZnSe nanosheet.

the non-polarized and non-magnetic nature of undoped structures. According to the structural symmetries and orbital overlap of s with p, see Fig. 6, the sp^2 hybridization has been formed. Broadening of these two orbitals (s and p) in the same range of energy confirms this result, as mentioned in [36]. In this monolayer form of ZnS and ZnSe, the sp^2–p bonding orbital is the total orbital that shows the overlapping of sp^2 hybridized orbital of S (Se) and Zn atoms with the p_z orbital of sulfur atoms.

3.3. Electronic and magnetic properties of doped ZnX monolayer

In order to investigate the magnetic properties of doped ZnS (ZnSe), first principle calculations were performed for all doped structures. The goal is to find 100% spin polarized materials. These types of materials have two necessary conditions that must be met simultaneously: (i) they have a magnetization with an integer number of Bohr magneton μ_{B}, (ii) an energy gap in only one of its spin channels, which confirms the half-metallic feature. Since the spins of the conducting band cannot easily flip to the valance band, the larger energy gap results in the better polarization quality of the material. With these two conditions, we try to introduce the half-metallic materials that have 100% polarization and are widely used in spin valves and spintronic manufacturing.

The fully relaxed lattice constant of ZnS and ZnSe monolayers is 3.822 Å and 3.980 Å, respectively. Doping atoms in ZnS and ZnSe are introduced by replacing a single host atom in the pristine system. In this paper, we mainly consider the transitional metal atoms as impurities to substitute instead of the host Zn, S or Se atoms. In one of the configurations, for the doped ZnS, the Zn atom is replaced by an impurity atom, represented as $Zn_{15}YS_{16}$ (Y = Fe, Co, Mn, Ni) in each supercell. In the other, for the doped ZnS, the S atom is replaced by an impurity atom, represented

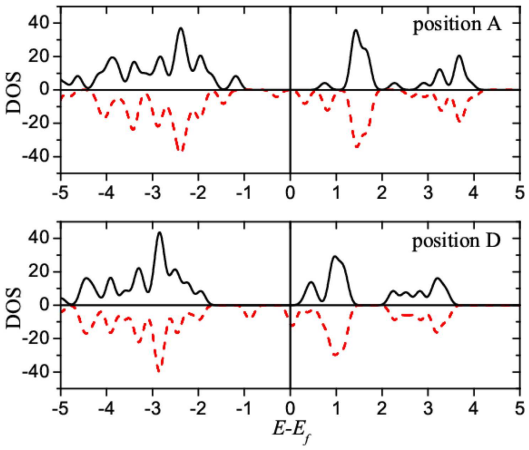

Fig. 7. Densities of states of the Fe-doped ZnS monolayer in two positions, black solid and red dashed lines, are related to spin up and spin down states, respectively.

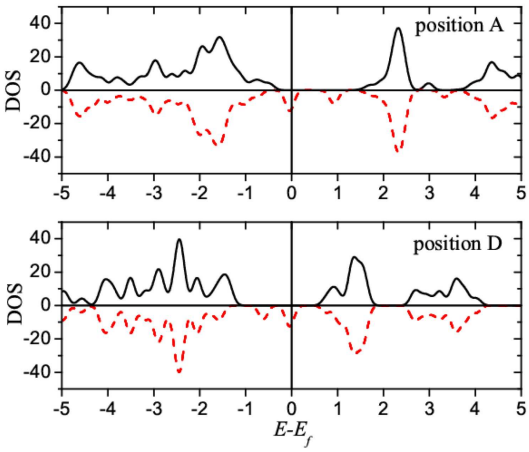

Fig. 8. Densities of states of Co-doped ZnS monolayer in two positions, black solid and red dashed lines, are related to spin up and spin down states, respectively.

as $Zn_{16}S_{15}Y$ (Y = Fe, Co, Mn, Ni). Also, the two configurations for the doped ZnSe are presented, including $Zn_{15}YSe_{16}$ and $Zn_{16}Se_{15}Y$ by replacing the Zn and Se atoms, respectively.

Figure 7 shows the DOS of the Fe-doped ZnS structure (S and Zn substitution). The graphs show that in the two configurations, in the upper spin channel there is a band gap around the Fermi energy. The values of these energy gaps are given in Table I. The graphs also show that in the A position, the density of states in the spin down channel at the Fermi energy level is much lower than in the D positions where the S atoms are replaced by the Fe atoms in the monolayer and we see a stronger polarization in the D positions. According to Table I, the amount of the energy gap in position D is larger than the other and shows the significant value of 1.536 eV. Also, the total magnetization due to the presence of Fe atoms in the structure is 4 μ_B for A and 2 μ_B for the D positions and hence all of these systems are ferromagnetic. Although the total magnetization of A position is larger than D, due to the significant asymmetric DOS in D, the polarization is stronger due to the larger asymmetry in its DOS. In these configurations, the largest deformation is related to the Fe atom which can be found from visualizing the optimized structure. This deformation, in fact, removes the degeneracy of the 3*d* orbitals of the Fe atom, and leads to the formation of the localized hydride states near the valance bands. As expected, the Fe dopant is the main contributor to the total magnetic moment [13].

We observed similar results over using Co impurity, see Fig. 8. Different levels of asymmetry and spin splitting occur in this doping structure and result in ferromagnetism property. The DOS of the spin up electron near the Fermi level is zero, which shows that this spin direction has a semiconducting character. With doping Co as an impurity, the DOS at the spin down at the Fermi level is significant, although the half-metallic energy gap is smaller than Fe-doped structures. However, the D configuration shows stronger polarization with a wider gap compared to the A configuration. The magnetization for A configuration is 3 μ_B and for D configuration is 1 μ_B (Table I). The results are in qualitative agreement with some results in [37].

Unlike the Fe case, the strong interaction between the Co and Zn or Co and S pairs leads to the formation of a localized impurity state near the valance bands. The reduction in the magnetic moment can be attributed to the pairing of the electrons in this mixed orbital. In other words, the magnetic properties of the Co-doped system depend on the competition between the ligand field splitting and the Hund coupling [38].

Unexpectedly, different results are obtained when Ni and Mn atoms are doped in ZnS. As can be seen in Fig. 9, these structures do not have any half-metallic properties, rather they show a semiconductive behavior (i.e., a significant bandgap). Table I shows the calculated total magnetization for these compounds. The spin up and spin down channels in the D position of the Ni-doped structure are entirely symmetric. According to the zero value of magnetization for Ni in the D configuration, this compound shows a non-magnetic semiconductor structure. In the other configuration (A), the total magnetic moment of the pure nanosheet increases to 2 μ_B, due to doping the Ni atom but with a very low level of polarity. During our calculations, we found that the $Zn_{15}MnS_{16}$ and $Zn_{15}MnSe_{16}$ compounds in configuration A have a high order of the net magnetic moment of 5 μ_B. Since one of the two necessary conditions of half-metallicity is not observed in other three positions, they are not half-metals but are magnetic semiconductors [39].

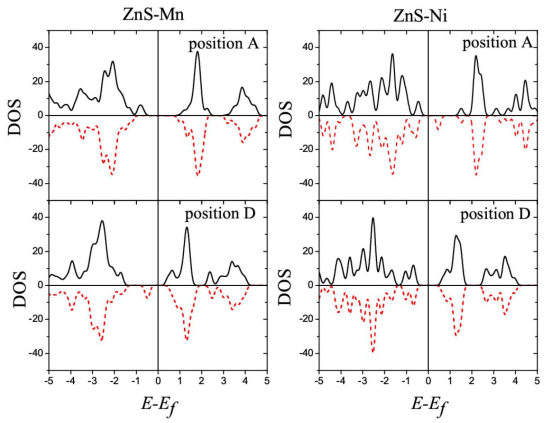

Fig. 9. Densities of states of Ni- and Mn-doped ZnS monolayers, black solid and red dashed lines, are related to spin up and spin down states, respectively.

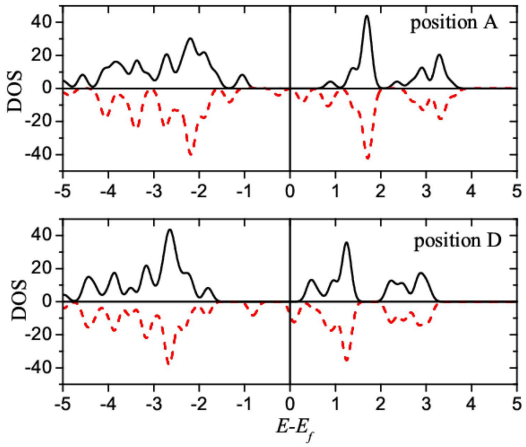

Fig. 10. Densities of states of Fe-doped ZnSe monolayer in two positions, black solid and red dashed lines, are related to spin up and spin down states, respectively.

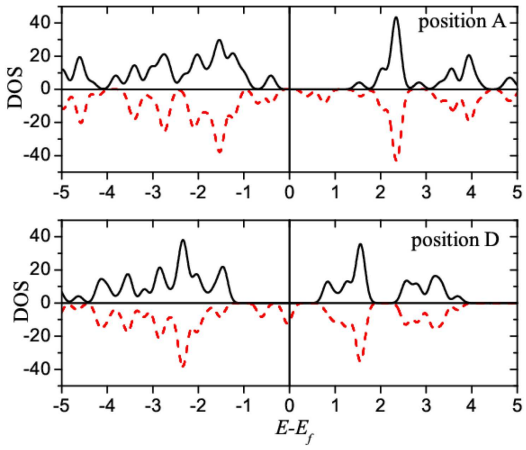

Fig. 11. Densities of states of Co-doped ZnSe monolayer in two positions, black solid and red dashed lines, are related to spin up and spin down states, respectively.

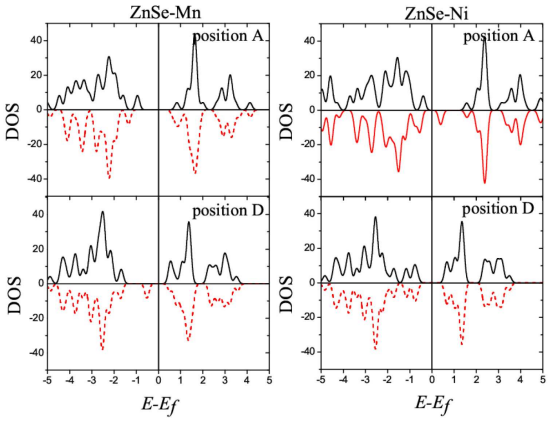

Fig. 12. Densities of states of Mn- and Ni-doped ZnSe monolayers in two positions, black solid and red dashed lines, are related to spin up and spin down states, respectively.

All of the calculations related to the ZnS monolayers with the impurities of Fe, Co, Mn and Ni in two positions A and D are repeated for the ZnSe monolayers. All the explanations mentioned above for the structure of ZnS can be repeated for the structure of ZnSe. For the Fe-doped ZnSe, similar results as for the ZnS structure are obtained and the half-metallic energy gap in these positions is slightly smaller. The total magnetization did not change, see Fig. 10. Half-metallic properties have been observed for the D configuration with more stable polarization.

In Fig. 11, the DOSs of Co-doped ZnSe are presented for two spin channels and many changes are observed as compared to the ZnS monolayer. When the Co atom is doped in the ZnS monolayer, both positions, A and D, show magnetic properties but the half-metallic property is seen only in the D position, and there exists a magnetic semiconductor property in the A position. Although this structure has an integer magnetic moment greater than 1 μ_B, it does not have 100% polarization and cannot be counted as a half-metal.

Since in Mn- and Ni-doped ZnSe monolayers, for both spin up and spin down channels, there is an energy gap, they do not show the half-metallic property and are considered as semiconductor, see Fig. 12. Similar to the D position of Ni-doped ZnS, also the total magnetization of Ni-doped ZnSe is zero and the system is not magnetized. In Fig. 13, the diagrams of total magnetization against the contribution of the supercell atoms containing the D position are plotted for all impurities in the ZnS monolayer. As shown, the total magnetization entirely belongs to the doping atoms and other atoms have no role in magnetization. On the other hand, according to the orbital structure and partial density of states related to the impurity

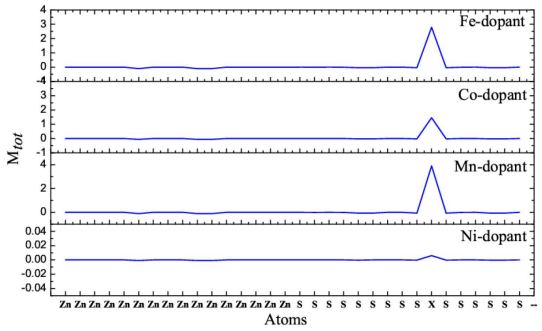

Fig. 13. Total magnetization of ZnS-X (X = Fe, Co, Mn and Ni), or X-doped ZnS, where doping atoms are put on the D positions.

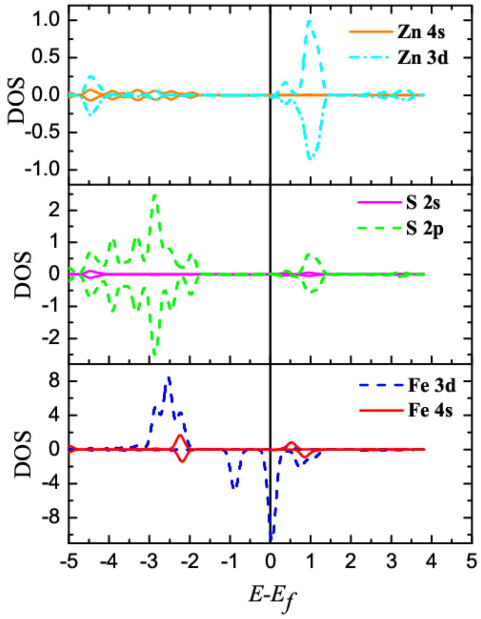

Fig. 14. Partial DOS of the Zn, S and Fe atoms in the ZnS-Fe supercell in the D position.

atom, there are extra electrons that contribute to total magnetization. For example, there are four electrons in the d orbital of the Fe atom which play the main role in magnetic property. Therefore, this argument can be generalized to other TM impurities, and the magnetic strength changes according to the number of free electrons in the d layer.

The magnetic properties mainly depend on the correlation between the defective bands. On the other hand, due to partial DOS of ZnS-Fe (as an example) in the D position (see Fig. 14), magnetic property is mainly related to the 3d orbital of the Fe atom rather than others. One can guess that the interaction between four free electrons of the d orbital leads to a spin cloud and induced magnetic properties in the structure. This description can be generalized to other structures. In other words, because of the coupling between the d orbital of the unsaturated Zn atoms and orbitals of the impurity atom, ZnS-Fe possesses a net magnetic moment.

4. Summary

In this work, the geometrical structure, formation energy, electronic and magnetic properties of Fe, Co, Mn and Ni doped in two positions of a hexagonal monolayer slab of ZnX (X = S, Se) were investigated by first principles calculations. All of the structures are stable. Our results show, when the Fe atom is doped in ZnS or ZnSe monolayer as an impurity in place of Zn or S (Se), that the structures possess a half-metallic property. When we doped the Co atom in both positions of the ZnS and ZnSe structures, it was observed that in both ZnS structures (A and D) and only in the D position of the ZnSe monolayer (where we replace the Se atom), the half-metallic property was observed. These structures have 100% polarization and are useful for spintronic applications. In other cases, semiconductor properties can be seen, although they also have magnetic properties. However, when the Mn and Ni atoms were used as doping impurities in the structures, the compounds became semiconductor and they could not be recommended for applications in the spintronic applications as a half-metallic material. The presented results can serve as useful hints for experimental efforts.

References

[1] K.S. Novoselov, A.K. Geim, S.V. Morozov, D. Jiang et al., *Science* **306**, 666 (2004).

[2] A.K. Geim, K.S. Novoselov, *Nat. Mater.* **6**, 183 (2007).

[3] Y.S. Ardakani, M. Moradi, *Eur. Phys. J. B* **93**, 99 (2020).

[4] Y.S. Ardakani, M. Moradi, *Phys. Solid State* **62**, 1262 (2020).

[5] M. Hernaez, *Sensors* **20**, 3196 (2020).

[6] K.S. Novoselov, V.I. Fal'ko, L. Colombo, P.R. Gellert, M.G. Schwab, K. Kim, *Nature* **490**, 192 (2012).

[7] F. Schwierz, *Nat. Nanotechnol.* **5**, 487 (2010).

[8] Q.H. Wang, K. Kalantar-Zadeh, A. Kis, J.N. Coleman, M.S. Strano, *Nat. Nanotechnol.* **7**, 699 (2012).

[9] B. Višić, *Nanomater. Energy* **4**, 18 (2015).

[10] Q. Ta. Huy, L. Zhao, D. Pohl, J. Pang, B. Trzebicka, B. Rellinghaus, D. Pribat, T. Gemming, Z. Liu, A. Bachmatiuk, M.H. Rümmeli, *Crystals* **6**, 100 (2016).

[11] B. Radisavljevic, A. Radenovic, J. Brivio, V. Giacometti, A. Kis, *Nat. Nanotechnol.* **6**, 147 (2011).

[12] W. Kohn, A.D. Becke, R.G. Parr, *J. Phys. Chem.* **100**, 12974 (1996).

[13] Cuifang Jia, Bo Zhou, Qi Song, Xiaodong Zhang, Zhenyi Jiang, *RSC Adv.* **8**, 18837 (2018).

[14] X.L. Fan, Y.R. An, W.J. Guo, *Nanoscale Res. Lett.* **11**, 154 (2016).

[15] M.D. Xie, C.G. Tan, P. Zhou, J.G. Lin, L.Z. Sun, *RSC Adv.* **7**, 20116 (2017).

[16] F. Zou, L. Zhu, G. Gao, M. Wu, K. Yao, *Phys. Chem. Chem. Phys.* **18**, 6053 (2016).

[17] A. Ramasubramaniam, D. Naveh, *Phys. Rev. B: Condens. Matter Mater. Phys.* **87**, 195201 (2013).

[18] Y.C. Cheng, Z.Y. Zhu, W.B. Mi, Z.B. Guo, U. Schwingenschlögl, *Phys. Rev. B: Condens. Matter Mater. Phys.* **87**, 100401 (2013).

[19] Q. Yue, S. Chang, S. Qin, J. Li, *Phys. Lett. A* **377**, 1362 (2013).

[20] M. Luoa, B. Yua, Y.H. Shen, *Acta Phys. Pol. A* **135**, 391 (2019).

[21] H. Zheng, B. Yang, D. Wang, R. Han, X. Du, Y. Yan, *Appl. Phys. Lett.* **104**, 132403 (2014).

[22] Y. Tian, Z. Zhu, Z. Ge, A. Sun, Q. Zhang, S. Huang, J. Meng, *Physica E: Low Dimens. Syst. Nanostruct.* **116**, 113745 (2019).

[23] Y. Zhao, W. Wang, C. Li, Y. Xu, L. He, *Solid State Commun.* **281**, 6 (2018).

[24] Y. Yang, X.L. Fan, R. Pan, W.J. Guo, *Phys. Chem. Chem. Phys.* **18**, 10152 (2016).

[25] H. Pan, *J. Phys. Chem. C* **118**, 13248 (2014).

[26] C. Jiang, Y. Wang, Y. Zhang, H. Wang, Q. Chen, J. Wan, *J. Phys. Chem. C* **122**, 21617 (2018).

[27] Z.K. Heiba, M.B. Mohamed, *J. Inorg. Organomet. Polym. Mater.* **30**, 879 (2020).

[28] M. Moradi, A. Mohammadi, M. Afshari, Z. Soltani, *J. Magn. Magn. Mater.* **332**, 81 (2013).

[29] M. Wu, Z. Wei, W. Zhao, X. Wang, J. Jiang, *J. Nanomater.* **2017**, 1 (2017).

[30] L.L. Kulyuk, R. Laiho, A.V. Lashkul et al., *Physica B* **405**, 4330 (2010).

[31] A.D. Lad, C. Rajesh, M. Khan, N. Ali, I.K. Gopalakrishnan, S.K. Kulshreshtha, S. Mahamuni, *J. Appl. Phys.* **101**, 103906 (2007).

[32] X. Zeng, J. Zhang, F. Huang, *J. Appl. Phys.* **111**, 123525 (2012).

[33] P. Giannozzi, S. Baroni et al., *J. Phys.: Condens. Matter* **21**, 395502 (2009).

[34] J.P. Perdew, K. Burke, M. Ernzerhof, *Phys. Rev. Lett.* **77**, 3865 (1996).

[35] S. Rodríguez, C. Zandalazini, J. Navarro, K.T. Vadiraj, E.A. Albanesi, *Mater. Res. Express* **7**, 016303 (2020).

[36] M. Jafari, Kh. Alvani, *Mater. Res. Express* **6**, 0850b5 (2019).

[37] R. Chaurasiya, A. Dixit, in: *The Physics of Semiconductor Devices, IWPSD 2017* Springer Proceedings in Physics, Vol 215. Springer, Cham 2019, p. 49.

[38] L.-B. Shi, J.-J. Liu, Y. Fei, *Physica B* **426**, 45 (2013).

[39] R.A. de Groot et al., *Phys. Rev. Lett.* **50**, 2024 (1983).